BBA - Biomembranes 1864 (2022) 183983

Contents lists available at ScienceDirect

BBA - Biomembranes

journal homepage: www.elsevier.com/locate/bbamem

Binding of DEP domain to phospholipid membranes: More than just electrostatics

Francesco L. Falginella [a,b], Marek Kravec [c], Martina Drabinová [a], Petra Paclíková [c], Vítězslav Bryja [c,d], Robert Vácha [a,b,e,*]

[a] CEITEC – Central European Institute of Technology, Masaryk University, Kamenice 5, 625 00 Brno, Czech Republic
[b] National Centre for Biomolecular Research, Faculty of Science, Masaryk University, Kamenice 5, 625 00 Brno, Czech Republic
[c] Department of Experimental Biology, Faculty of Science, Masaryk University, Brno 62500, Czech Republic
[d] Institute of Biophysics, Academy of Sciences of the Czech Republic, v.v.i., Brno 612 65, Czech Republic
[e] Department of Condensed Matter Physics, Faculty of Science, Masaryk University, Kotlářská 2, 611 37 Brno, Czech Republic

ARTICLE INFO

Keywords:
DVL protein
DEP domain
Lipid membrane
Molecular dynamics
Flow cytometry
QCM-D
Lipid preference
Phosphatidylserine
Phosphatidic acid
Phosphatidylinositol

ABSTRACT

Over the past decades an extensive effort has been made to provide a more comprehensive understanding of Wnt signaling, yet many regulatory and structural aspects remain elusive. Among these, the ability of Dishevelled (DVL) protein to relocalize at the plasma membrane is a crucial step in the activation of all Wnt pathways. The membrane binding of DVL was suggested to be mediated by the preferential interaction of its C-terminal DEP domain with phosphatidic acid (PA). However, due to the scarcity and fast turnover of PA, we investigated the role on the membrane association of other more abundant phospholipids. The combined results from computational simulations and experimental measurements with various model phospholipid membranes, demonstrate that the membrane binding of DEP/DVL constructs is governed by the concerted action of generic electrostatics and finely-tuned intermolecular interactions with individual lipid species. In particular, while we confirmed the strong preference for PA lipid, we also observed a weak but non-negligible affinity for phosphatidylserine, the most abundant anionic phospholipid in the plasma membrane, and phosphatidylinositol 4,5-bisphosphate. The obtained molecular insight into DEP-membrane interaction helps to elucidate the relation between changes in the local membrane composition and the spatiotemporal localization of DVL and, possibly, other DEP-containing proteins.

1. Introduction

Wnt signaling arguably represents one of the most evolutionary conserved signaling pathways in the whole animal kingdom and it is known to regulate cell fate and growth during embryonic development and tissue homeostasis. From a clinical perspective, its deregulation was shown to be linked with the onset and progression of various types of cancer [1–3]. After the pathway initiation by the interaction of the Wnt ligands with Frizzled (FZD) transmembrane receptors, the association to the plasma membrane of Dishevelled (DVL) protein constitutes an early cytoplasmic event in both canonical (β-catenin dependent) and non-canonical (β-catenin independent) Wnt responses [4–6].

The human genome encodes three DVL isoforms (DVL 1,2,3), all containing three highly conserved domains: an amino-terminal DIX (dishevelled, axin) domain, a central PDZ (postsynaptic density 95, discs large, zonula occludens-1) domain, and a carboxyl-terminal DEP (dishevelled, Egl-10, pleckstrin) domain [7]. DEP domain is essential for the capacity of DVL to transduce Wnt signal [8,9] and it mediates its recruitment to the plasma membrane by two at least partially distinct mechanisms: (1) protein-protein interaction with transmembrane Frizzled receptor [10,11] and (2) the direct association with lipid molecules. The latter was suggested to be controlled by the electrostatic attraction existing between positively charged residues on the domain and negatively charged phospholipids, with a strong propensity for phosphatidic acid (PA) [12–14]. However, the molar concentration of PA in the inner leaflet of the plasma membrane is generally very low compared to other

Abbreviations: DVL, Dishevelled; PA, phosphatidic acid; PS, phosphatidylserine; PIP2, phosphatidylinositol 4,5-bisphosphate; PC, phosphatidylcholine; PG, phosphatidylglycerol.

* Corresponding author at: CEITEC – Central European Institute of Technology, Masaryk University, Kamenice 5, 625 00 Brno, Czech Republic.
E-mail address: robert.vacha@muni.cz (R. Vácha).

https://doi.org/10.1016/j.bbamem.2022.183983
Received 5 January 2022; Received in revised form 6 May 2022; Accepted 31 May 2022
Available online 21 June 2022

phospholipids [15,16], such as the negatively charged phosphatidylserine (PS) and the neutral phosphatidylcholine (PC) and phosphatidylethanolamine (PE). It remains unclear how these more abundant lipids influence DEP domain association with the membrane.

All-atom Molecular Dynamics (MD) simulations of DEP domain at model membranes composed of PA, PS, PE, PC, and phosphatidylglycerol (PG), a negatively charged lipid from mitochondria and bacteria (see Fig. 1), were performed to investigate the role of electrostatics in DEP-membrane interaction. The in silico results were complemented by flow cytometry measurements and quartz crystal microbalance with dissipation monitoring (QCM-D), which verified the membrane association of both DEP domain and full DVL with lipid vesicles and supported lipid bilayers of similar composition. The obtained lipid specificity of the DEP-membrane interaction sheds light on the mechanisms involved in the regulation of Wnt signaling and general membrane association of DEP domain containing proteins [17].

2. Methods

2.1. Simulated systems

We investigated the interaction of DEP domain with membranes of the following lipid compositions (in molar ratios): POPA, POPC, POPA:POPC (1:1), POPS:POPC (1:1), POPG:POPC (1:1), POPS:POPE:POPC (7:15:10), and POPS:POPA:POPC (1:1:2), where POPA is 1-palmitoyl-2-oleoyl-sn-glycero-3-phosphate, POPC is 1-palmitoyl-2-oleoyl-sn-glycero-3-phosphocholine, POPE is 1-palmitoyl-2-oleoyl-sn-glycero-3-phosphoethanolamine, POPS is 1-palmitoyl-2-oleoyl-sn-glycero-3-phospho-L-serine, and POPG is 1-palmitoyl-2-oleoyl-sn-glycero-3-phospho-(1′-rac-glycerol). POPS and POPG lipids had a net charge of −1e, while POPC and POPE were zwitterionic [18]. POPA lipid has pK_a close to neutral pH [19], thus in the case of POPA:POPC membrane, we simulated both singly and doubly deprotonated states of PA. For pure POPA membrane, only singly deprotonated lipids were considered due to the increased local pK_a at such highly charged surface [20]. Similarly, singly deprotonated POPA was also used in POPS:POPA:POPC membrane to enable a straight comparison between POPA and POPS lipids. All membranes were constructed by means of CHARMM-GUI membrane builder [21–23] and consisted of 64 lipids per leaflet. The membranes were then solvated with roughly 5000 water molecules and counter-ions for electroneutralization and equilibrated for at least 100 ns at 310 K and 1 bar. Note that in the case of POPC membrane, an identical sized equilibrated configuration was obtained from Slipids website.

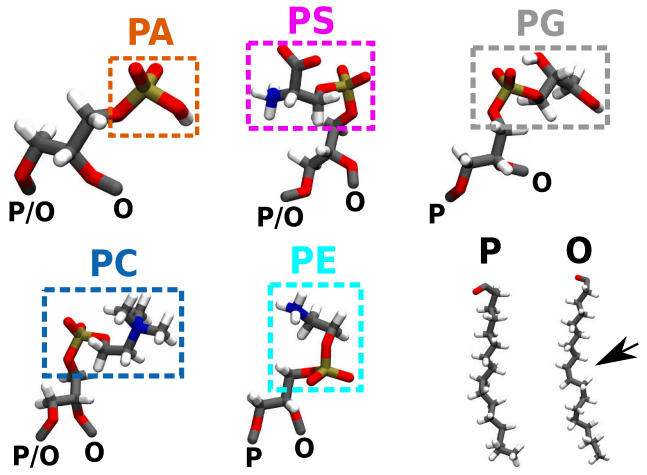

Fig. 1. Schematic representation of the studied phospholipids. For each lipid the polar headgroup (dashed box) and the glycerol are shown at atomistic detail. The palmitoyl (P) and oleoyl (O) acyl tails, shared by all lipids in the simulated systems, are shown at the bottom right of the figure. Note that in our experiments we investigated both singly and doubly unsaturated states of PA, PS, and PC lipids. Color code: red for oxygen, dark grey for carbon, white for hydrogen, blue for nitrogen, and tan for phosphorus. (For interpretation of the references to color in this figure legend, the reader is referred to the web version of this article.)

The structure of DEP domain from human DVL3 was modelled based on the crystal structure of DEP domain from mouse Dvl2 (PDB ID 3ML6 [24]), which has a high sequence identity (~90 %). The required mutations were performed manually using PyMOL [25].

One copy of the domain was then placed at approximately 1.5 nm from each leaflet of the equilibrated lipid bilayers. To mitigate the bias of the initial conditions, five different orientations of the domain were prepared such that the size of the positively charged surface patches oriented towards the membrane was progressively decreasing from orientation A to E of Fig. 2. The charge patches on the domain were determined based on its surface electrostatic potential calculated via the PDB2PQR server [26] and the Adaptive Poisson-Boltzmann Solver [27]. Note that the selected orientations included the previously identified [14] PA binding interface (Fig. 2A). Unlike the other systems, for DEP at POPS:POPE:POPC and POPS:POPA:POPC membranes, only this orientation was assessed. Finally, the systems were re-solvated with roughly 15,000 TIP3P [28] water molecules and about 150 mM NaCl ions were added with excess ions to neutralize the system charge.

2.2. Molecular dynamics simulations

The solvated DEP-membrane systems were first energy minimized to remove the sterical clashes. A two-step energy minimization (with and without harmonic restraints) was performed using the steepest descent algorithm until the maximum net force was <500 or 1000 kJ mol^{-1} nm^{-1}. Harmonic restraints with a force constant of 1000 kJ mol^{-1} nm^{-2} in each spatial direction were applied to all protein heavy atoms and all lipid atoms. After minimization, the systems were heated for 4 ns to 310 K in the NVT ensemble with harmonic restraints on all protein heavy atoms. Subsequently, three NPT ensemble steps of 1 ns each, were performed with restraints sequentially applied on all protein heavy atoms, backbone, and Cα atoms. To study membrane bound conformations of DEP, the domain was slowly pulled (rate of 0.25 nm ns^{-1}) by its center-of-mass (COM) to the membrane surface. The pulling was performed over 9 ns with a force constant of 1000 kJ mol^{-1} nm^{-2}. After the pull, 5 ns of unrestrained NPT equilibration was performed to relax the system. Finally, 500 ns production run was carried out at 310 K and pressure of 1 bar.

During all simulations, the covalent bonds in both protein and lipid molecules were constrained using LINCS [29] algorithm, while the water molecules were kept rigid by SETTLE [30] algorithm. These constraints allowed us to use a time step of 2 fs. Periodic boundary conditions were applied in all directions. The van der Waals interactions were shifted to zero at 1.2 nm and long-range dispersion corrections for energy and pressure were applied. The long-range electrostatics was treated using the particle mesh Ewald method (PME) [31], with cubic interpolation and Fourier grid spacing of 0.12 nm, while the distance cutoff for the real-space PME contribution was 1.2 nm. The center-of-mass translation of the protein/bilayer group relative to the solvent was removed every 100 steps. The temperature was regulated using multiple velocity-rescaling thermostats [32] for the protein, membrane, and solvent groups, with coupling time of 0.1 ps and 1 ps for the equilibration and production run, respectively. The pressure was controlled by the Parrinello-Rahman barostat [33] with semiisotropic scheme using coupling time of 5 ps for the equilibration and 10 ps for the production run.

To quantitatively evaluate how the DEP-membrane association is affected by changes in the overall charge of the membrane, the nature of the anionic lipids, and their specific concentration, we calculated the free energy of binding of DEP domain to the following membranes (with mol:mol ratios): POPA, POPC, POPA:POPC (1:1), POPS:POPC (1:1), and

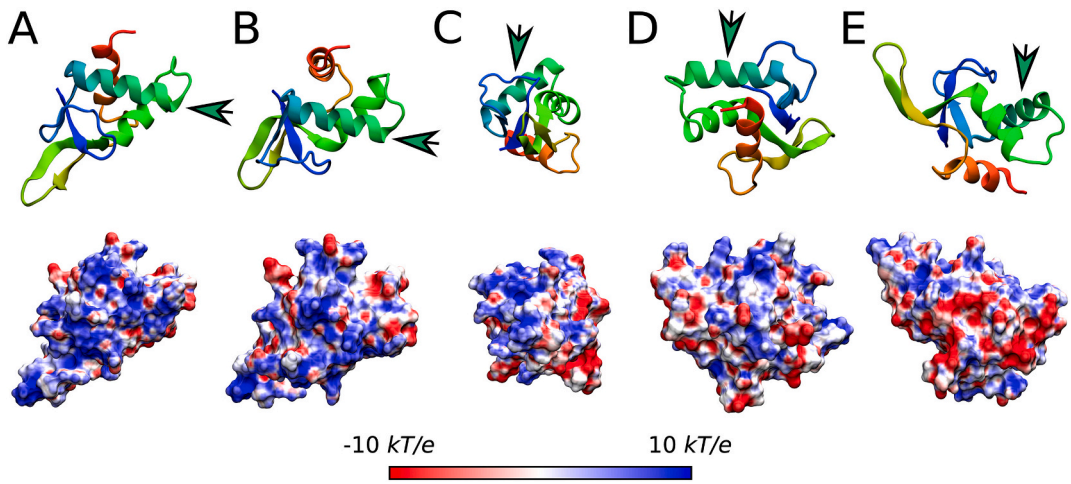

Fig. 2. Five different starting orientations of DEP domain were evaluated for their membrane binding ability (A–E). *Upper Panels)* Cartoon representation of the domain, colored with a red-green-blue scale from N- to C-terminus. The green arrow indicates the position of Helix3, previously reported to interact with phosphatidic acid (PA) lipid via a cluster of positively charged residues. *Lower Panels)* Surface electrostatic potentials for the corresponding orientations displayed in the upper panels. In all cases, the protein side oriented towards the membrane is shown. Note that orientation A exposes to the membrane all residues critical for PA binding [14]. (For interpretation of the references to color in this figure legend, the reader is referred to the web version of this article.)

POPS:POPE:POPC (7:15:10) by means of the umbrella sampling method [34–36]. Starting from a membrane-bound configuration, each copy of the domain was slowly pulled away from the membrane using a force constant of 1000 kJ mol^{-1} nm^{-2} and a pulling rate of 0.25 nm ns^{-1}. The starting coordinates for each window were generated every 0.05 nm based on the distance between the center of mass (COM) of DEP domain and the COM of a local cylindrical region on the membrane. The cylinder had radius of 2.5 nm and its main axis, parallel to the membrane normal (z-axis), passed through the COM of DEP domain. After 100 ns equilibration, 150 ns long production run was performed for each window. The final umbrella sampling windows were analyzed via the weighted histogram analysis method (WHAM) [37]. To minimize the deformations of the protein fold during the pulling and in umbrella windows, dihedral restraints with a force constant of 500 kJ mol^{-1} rad^{-2} were applied on all backbone atoms. Additional positional restraints with a force constant of 1000 kJ mol^{-1} nm^{-2} were applied on all Cα atoms, restricting the motion of DEP domain in the membrane plane, i.e. xy-directions. Similarly, during the pulling, flat-bottomed position restraints with a force constant of 1000 kJ mol^{-1} nm^{-2} were used on all lipid heavy atoms, which suppressed membrane defects in the z-direction. The flat-bottomed position restraints were partially relaxed in all windows by including only the heavy atoms until the lipid carbonyl region.

All our Molecular Dynamics simulations and analysis were performed using GROMACS 5.x and 2016.4 packages [38,39], for classic MD and free energy calculation, respectively. Amber ff99SB-ILDN [40] parameters were used for DEP domain, whereas for lipid molecules we used Slipids [41–43] parameters. For POPA we built a new parameter set based on Slipids parametrization (see below for details). The POPS parameters were constructed by combination of the headgroup region from 1,2-dioleoyl-sn-glycero-3-phospho-L-serine (DOPS) lipid and the acyl tails from POPG lipid. Fig. S1 and Table S1 provide a comparison of the acyl chain order parameters and the area per lipid for equilibration (Charmm36) and production run (Slipids) simulations. All values are in good agreement with only the full POPA membrane simulated with the custom POPA model showing a slightly increased ordering. Note that for the equilibration simulations no DEP domain was present in the system. All the simulation input files can be found on Zenodo (DOI: https://doi.org/10.5281/zenodo.6505455).

2.2.1. POPA parametrizations

The bonded and non-bonded parameters for POPA lipid (singly and fully deprotonated) were based on the preexisting Slipids parametrization of the acyl tails, glycerol, and phosphate group structural blocks [41–43]. Note that for the terminal hydroxyl hydrogen of singly deprotonated POPA we used generic dihedrals parameters.

The partial atomic charges for the headgroup atoms were obtained as a Boltzmann average over an ensemble of representative conformations, as previously described [41,42]. Briefly, 26 lipid structures were chosen to maximize the structural diversity based on the Root Mean Square Deviation (RMSD) from a POPA membrane simulated (50 ns at 303 K) using CHARMM36 [44] force field. To reduce the computational cost, the hydrophobic region of each lipid was trimmed, discarding all atoms beyond the apolar carbon at position 3 in both acyl tails. The resulting molecules were energy minimized using the B3LYP functional form [45–47] and cc-pVTZ basis set [48]. The charges were computed applying the restricted electrostatic potential approach [49] (RESP) with an identical combination of DFT method and basis set. All solvent effects were accounted for using the IEFPCM continuum solvent model [50,51] with relative dielectric constant of 78.4. The computed electrostatic potential was fitted with the Merz-Singh-Kollman scheme [52]. To ensure an overall molecular charge of −1e and −2e, the resulting charge excess was redistributed among all atoms, with the exception of the phosphate group oxygens for which the quantum mechanical values were preserved (Tables S2 and S3). All quantum mechanical and RESP calculations were performed with Gaussian16 software package [53] and Antechamber tool [54,55], respectively.

2.3. Analysis of MD simulations

Several gromacs tools [38,39] were used with default parameters to perform routine analyses on the calculated trajectories. In particular, we (1) evaluated the overall stability of DEP domain (*gmx rms*), (2) determined the radial distribution function (RDF) between DEP molecular surface and the P atoms of the lipid phosphate groups in systems containing POPA:POPC, POPS:POPC, and POPG:POPC membranes (*gmx rdf*), and (3) calculated the mass density profile along the membrane normal of DEP and the structural components of each phospholipid type (*gmx density*). Four lipid components were examined: headgroup substituent (i.e. choline, serine, ethanolamine, and glycerol), phosphate group, glycerol backbone, and fatty acid tails. For simplicity the hydroxyl hydrogen of phosphatidic acid was considered part of the phosphate group rather than a separated headgroup substituent. VMD software [56] and its STRIDE plugin [57] were used to create all the

visualizations and predict the secondary structure of DEP, respectively.

2.3.1. Identification of DEP domain membrane binding site

The residues of DEP domain responsible for binding the lipid membranes were identified using three different indicators, averaged over all DEP copies and starting orientations. *Contacts:* per-frame number of contacts, where a contact is defined for each residue-lipid atom pair with distance lower than 0.3 nm (calculated using the *distances* collective variable from *plumed* plug-in [58]). The average value over the whole simulation is then reported for each protein residue. *Hydrogen Bonds:* sum of all hydrogen bonds formed by a protein residue with any lipid molecule. The hydrogen bonds were computed using *gmx hbond* with default parameters (i.e. angle Hydrogen-Donor-Acceptor $\leq 30°$ and distance Donor-Acceptor ≤ 0.35 nm). *Interaction Energy:* time-averaged short-range Coulombic and Lennard-Jones energy contributions for each residue-membrane interaction using the *rerun* option of *gmx mdrun*. We note that all three indicators were evaluated for the membrane as a whole and for each lipid component separately, as defined in the previous section.

2.3.2. DEP domain binding mode

Throughout our simulations we observed no major fluctuations of the atomic positions (Fig. S2) and/or changes in the secondary structure content (Fig. S3) of DEP domain, indicating that the overall fold was mostly unaffected by the interaction with the membrane. We thus approximated the domain as a rigid body and characterized the conformations of the bound domain using two intramolecular vectors described by the spatial coordinates of the Cα atoms from residues pairs 412–435 and 462–472, respectively (see Fig. S4). These atoms pairs were selected based on their low RMSF (Root Mean Square Fluctuations) values and the virtually orthogonal arrangement of the generated vectors. Finally, from the probability distribution of the cosine of the angles formed between each of the two vectors and the z-axis (membrane normal), the free energy surface (FES) was derived using $-kT \ln H(x)$, where $H(x)$ is the probability distribution and kT is the units factor with value 2.577483 kJ mol^{-1} at 310 K.

2.4. Experiments

2.4.1. Vesicles preparation

Lipid vesicles were prepared using six different phospholipids: POPA, POPS, POPC, 1,2-Dioleoyl-sn-glycero-3-phosphatidic acid (DOPA), 1,2-Dioleoyl-sn-glycero-3-phosphatidylserine (DOPS), and 1,2-Dioleoyl-sn-glycero-3-phosphocholine (DOPC) (Fig. 1). Together with the pure lipid vesicles, DOPA:DOPC and phosphatidyl inositol 4,5-biphosphate (PIP2):DOPC mixtures at, respectively, 1:1 and 1:3 M ratios were also tested. Aliquots of each lipid stock solution, all purchased from Avanti, were added to a glass vial, in the presence and absence of the lipophilic cationic indocarbocyanine dye, DiD (molar ratio of 2000:1 of phospholipid:DiD). The excess solvent was initially removed using a gentle stream of air, then the lipid films were fully dried overnight in a vacuum dessicator. The dried lipid films were pre-hydrated with a very small volume of MQ water in a hot water bath (~35 °C) for at least 5 min. Next, 500 μL of 50 mM Tris, pH 8, 150 mM NaCl, 1 mM EDTA were added to each lipid film to obtain a final lipid concentration of 200 μM. The samples were allowed to rest at least one night in a hot room (37 °C) before measurements.

2.4.2. Protein purification

Twin-Strep-Halo N-terminally tagged full-length DVL3 (aa1–716) or DEP domain (aa 389–496) was overexpressed in HEK293 cells using PEI transient transfection. Cells were harvested 48 h post-transfection, resuspended in a lysis buffer (50 mM Tris, pH 8, 150 mM NaCl, 10 % glycerol) supplemented with protease inhibitors cocktail (Roche) and 0.2 % NP40 (Sigma). The mixture was incubated for 20 min on ice and cell lysis was enhanced by sonication. Cell lysate was cleared by centrifugation at 40,000*g* for 1 h min at 4 °C and supernatant was loaded on Strep-Tactin Superflow high-capacity column (IBA lifesciences) equilibrated in the purification buffer (50 mM Tris, pH 8, 150 mM NaCl, 10 % glycerol). The column was washed in the purification buffer and the protein was eluted using purification buffer supplemented with 3 mM desthiobiotin. Eluted proteins were concentrated to 1 mg mL^{-1} using protein concentrators, 10 K MWCO (Thermo Fisher Scientific), and submitted to size-exclusion chromatography using Superdex 200 Increase 10/300 GL (Cytiva) column on ÄKTA pure Chromatography System (Cytiva) with the size exclusion buffer (50 mM Tris, pH 8, 150 mM NaCl, 1 mM EDTA). Individual fractions were analyzed by SDS PAGE. Fractions of the purest protein were pulled together and concentrated to 1 mg mL^{-1} using protein concentrators, 10 K MWCO (Thermo Fisher Scientific), flash frozen in liquid nitrogen, and aliquots were stored at −80 °C. Concentrations of proteins were measured on Nanodrop ND-1000 instrument (Peqlab). For HALO tag removal, HALO-DEP was incubated with TEV protease (in molar ratio TEV to protein 1:100) overnight at 4 °C. The next day, the solution was 10× diluted and loaded on Strep-Tactin Superflow highcapacity column (IBA lifesciences) equilibrated in the purification buffer (50 mM Tris, pH 8, 150 mM NaCl, 10 % glycerol) and flow-through fraction was collected. Protein was subsequently concentrated to 3 μM using protein concentrators 10 K MWCO (Thermo Fisher Scientific) and transferred to the buffers used for QCM measurements using Zeba Spin Desalting Columns, 7 K MWCO, 0.5 m (Thermo Scientific).

2.4.3. Protein-vesicles binding assay

As mentioned above, lipid vesicles were labelled with DiD fluorescent dye, while the protein staining was performed as follows. After thawing of protein aliquot, the sample was spun down 20,000 *g*, at 4 °C for 15 min to remove any possible aggregates. Then, a fluorescent HaloTag TMR Ligand (Promega) and the recombinant protein were incubated for 20 min at 4 °C in final concentrations of 30 μM TMR ligand and 10 μM protein. The unbound ligand was removed by buffer exchange step using Zeba Spin Desalting Columns, 7 K MWCO, 0.5 m (Thermo Scientific). The protein was transferred to the same buffer that was used for preparation of vesicles to avoid any osmotic stress. To obtain clear membrane binding we needed to use about an order of magnitude higher concentration of DEP domain compared to full-length DVL3. Finally, the protein was equilibrated and then incubated with lipid vesicles in ratio 2:1 (total volume 9 μL) for 15 min at room temperature (vesicles with DO lipids) or 37 °C (vesicles with PO lipids). Then the mixture of vesicles and protein was diluted to working concentration (defined by event rate in flow cytometry measurements of control samples) by the same buffer and the samples were analyzed using spectral flow cytometer Northern Lights 3000 (Cytek). All buffers were filtered using 0.22 μm Millex-GV Syringe Filter Unit (Millipore) prior to use.

2.4.4. Flow cytometry

Comparison of stained and unstained lipid vesicles together with 0.22 μm filtered buffer control was used to determine the gating strategy for vesicles and to exclude noise. Samples were diluted to provide real-time event rate between 1000 and 2000 total events per second and abort rate under 50 events per second. Flow rate was set to 30 μL min^{-1} for PC vesicles and 15 μL min^{-1} for the other vesicles. For the DiD gate, 10,000 events were recorded per each sample (100,000 events in case of PIP2:DOPC vesicles). Fluorescence signals in the channel R2, corresponding to DiD vesicular staining, and B4, corresponding to TMR protein staining, were analyzed and fluorescence intensities for recorded events are shown as histograms (see Fig. S5A-L). Overlay of histograms from control vesicles and vesicles incubated with protein samples represents binding of protein to the vesicles as a shift in fluorescence intensity for recorded events. All flow cytometry figures were generated using NovoExpress Software (Agilent).

2.4.5. SDS PAGE

Protein samples from vesicle–protein binding assay were mixed with 2× sampling buffer in 1:1 ratio and incubated at 95 °C for 5 min. Then the proteins were separated on SDS-PAGE using 8 % polyacrylamide gels. Gels were fixed with 10 % acetic in 30 % methanol/MQ water and stained with Coomassie brilliant blueR-250 for 1 h. Subsequently, gels were destained in the fixing solution.

2.4.6. Confocal microscopy

150 μL of 200 μM lipid vesicles sample was mixed with 15 μL of either TMR stained HALO-DVL3 or HALO-DEP protein (see Protein-Vesicles Binding Assay) and control sample was mixed with the same amount of control buffer. The mixture was gently pipetted into μ-Slide 8 Well (Ibidi) chamber and the slider was let to rest for 15 min at room temperature. Subsequently, pictures were taken by confocal microscope (Leica SP8) using 40× water objective.

2.4.7. Quartz crystal microbalance with dissipation (QCM-D) monitoring

The binding of DEP domain (with and without HaloTag TMR Ligand) to DOPC, DOPA:DOPC (1:1 mol:mol), DOPS:DOPC (1:1 mol:mol), and PIP2:DOPC (1:3 mol:mol) supported lipid bilayers (SLBs) was independently assessed via QCM-D experiments. All measurements were performed on device QSense Analyzer (Biolin Scientific, Sweden) using SiO_2 sensors (QSX 303, Biolin Scientific, Sweden). Solvent-assisted lipid bilayer formation method [59] with ethanol (Avantor, USA) and the buffer from the protein purification (50 mM Tris, pH 8, 150 mM NaCl, 1 mM EDTA) was used to create the SLBs on sensors. Lipids dissolved in chloroform (Avanti, USA) were mixed in a round bottom test tube, dried under a gentle stream of air, and kept under vacuum for 4 h. Then ethanol was added to create lipid concentration in ethanol of 0.2 mg mL^{-1}. During measurement, flow rate was set to 50 μL min^{-1}. The protein was injected after stable SLBs were observed for at least 5 min.

3. Results

3.1. Electrostatics-driven membrane binding

Our 500 ns long MD simulations showed that DEP domain is able to interact with all the anionic membranes investigated, regardless of their composition and nature of the lipid molecules (see Figs. 3 and S6). Even the lowest content of negatively charged lipids (~22 %) was sufficient for a stable binding, and only when the membrane had net zero charge (pure POPC), the domain desorbed (Figs. 3 and S6 - bottom row). To capture the membrane binding, we calculated the mass density profile (along the membrane normal) of DEP domain and the structural components of each phospholipid type, averaged over all simulations (see Methods). As anticipated, for membranes containing anionic lipids, the peak of DEP domain was located in the proximity of the membrane surface, while for pure POPC membrane, the weaker interaction resulted in a broader peak, with a non-zero tail in the bulk solution (see Fig. S7). Moreover, we observed that in all cases the domain and the phosphate groups interacted at similar distance, with the exception of the membrane with doubly deprotonated POPA (see Table S4). This same separation, i.e. depth of DEP insertion in the membrane, suggests that the direct interaction between the lipid phosphate groups and DEP domain plays a key role in DEP-membrane binding.

3.2. Binding mode

The protein amino acids responsible for the association with the lipid membranes were identified based on the (1) contacts, (2) hydrogen bonds, and (3) strength of the interaction energy (see Methods for details). Taken collectively, the analysis from all indicators suggests that three separate protein regions, rich in positively charged amino acids, are implicated in binding the membrane (Figs. S8 to S10): the tip of DEP finger (residues 434-LKI-436), Helix 3 (residues 462-REARKYASNLL-KAG-475), and a contiguous loop (residues 482-NKITFSEQ-489). In addition, few basic (i.e. R429 and R431) and non-polar (i.e. M432, I436, and W433) residues flanking the DEP finger stabilized its binding to the membrane by occasionally interacting with the lipids. A condensed view of the interaction energies of the identified regions and the rest of the domain is depicted in Fig. 4. For POPC membrane, from which the domain desorbed during the simulation, the energies are exceptionally weak. In contrast, membrane with doubly deprotonated POPA showed a unique distribution of interactions indicating a distinct binding mode. Consistent results, especially the lack of interactions between DEP and the neutral POPC membrane (see Figs. S11 to S14), were obtained in simulations starting from configurations with the domain in solution

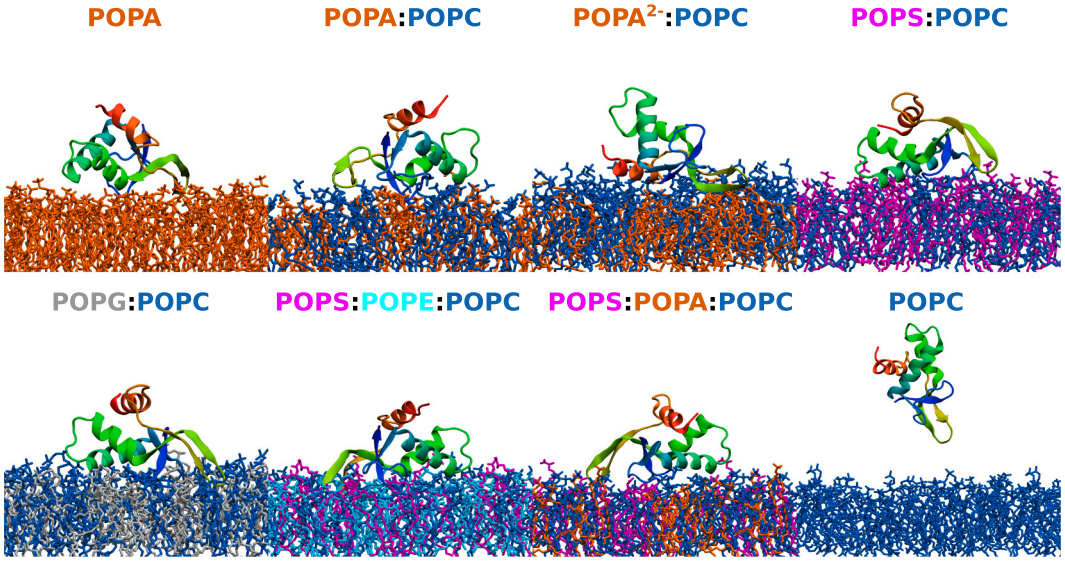

Fig. 3. Representative snapshots from 500 ns long all-atom simulations of DEP domain interacting with different phospholipid membranes. DEP domain was steadily bound to all studied anionic membranes, while the weak interaction with the neutral POPC bilayer occasionally led to desorption. The domain representation is the same as in Fig. 2. The phospholipids heavy atoms are displayed in 'licorice' and are colored as follows: dark-orange for POPA (singly and doubly deprotonated), blue for POPC, cyan for POPE, magenta for POPS, and grey for POPG. Ions and water molecules are omitted for clarity. (For interpretation of the references to color in this figure legend, the reader is referred to the web version of this article.)

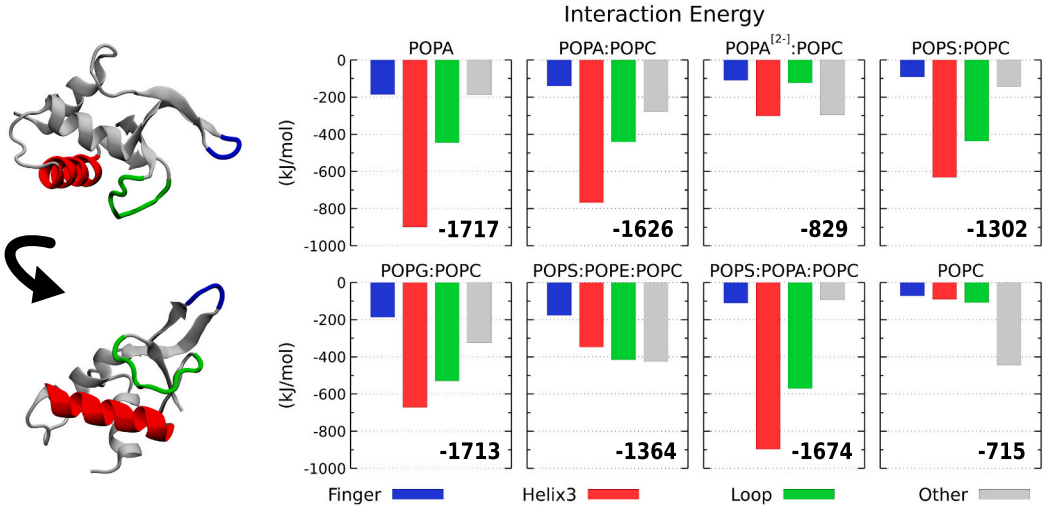

Fig. 4. Protein regions critical for DEP-membrane binding. The leftmost panels show rotated views of DEP domain highlighting the location of the DEP finger (blue), Helix 3 (red), and the contiguous loop (green). The bar plots on the right side of the figure display the interaction energy for each of the important DEP region along with the contribution of the remaining residues of DEP domain (colored in grey to match the views on the left). The total interaction energy is also shown for each DEP-membrane system. (For interpretation of the references to color in this figure legend, the reader is referred to the web version of this article.)

(Fig. S15).

In agreement with the density distribution analysis, most of the hydrogen bonds and interaction energy of the bound domain with the membranes, originate from the lipid phosphate groups irrespective of the headgroup type (red bars in Figs. S9 and S10), and were predominantly driven by electrostatics (see Figs. S16 and S17).

The large fluctuations observed in the time evolution of the protein-membrane contacts (Fig. S6) and the used per-residue indicators (Tables S5 to S7), suggest variability in the domain binding mode. Therefore, for each system we analyzed the orientations sampled by the domain (see Methods for details). The obtained free energy surface (FES) displayed a similar landscape for all bound domains, with the local

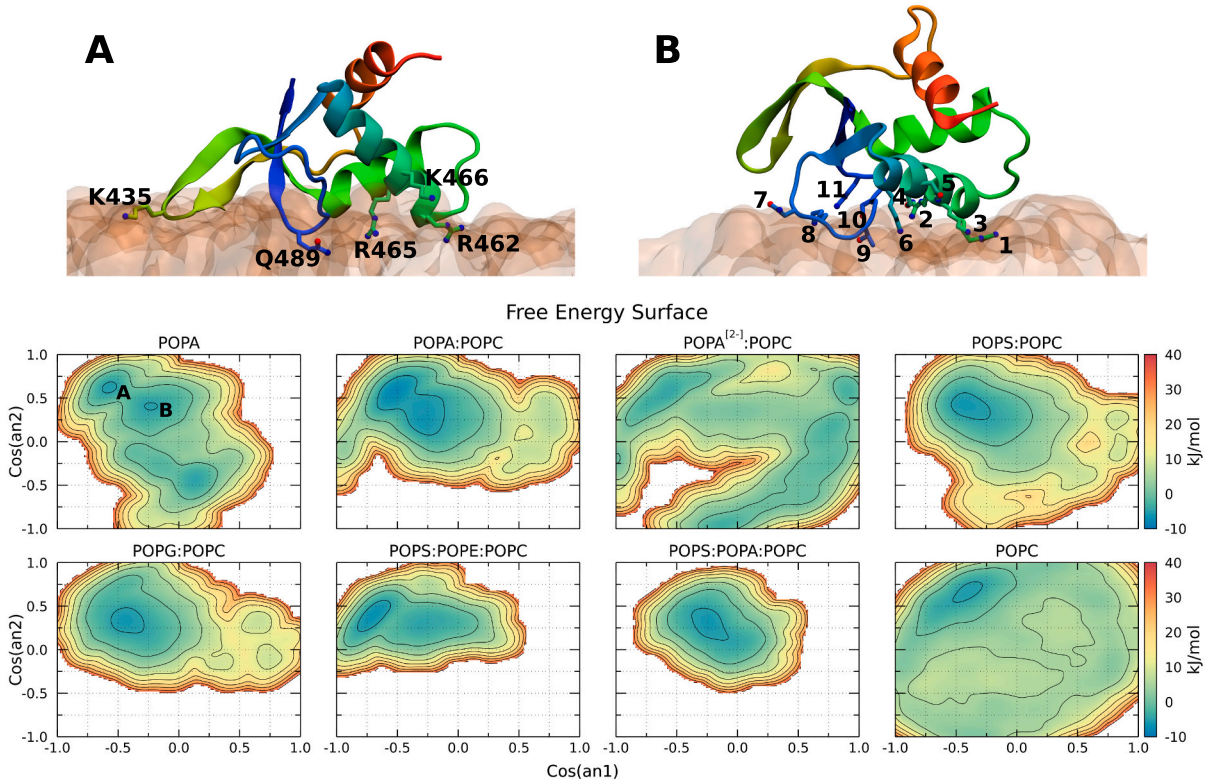

Fig. 5. Characterization of the different binding modes. Bottom plots: Free energy surface reconstructed based on the distribution of the binding orientations sampled by DEP domain. For DEP at POPA membrane, we highlighted the position of the local minima corresponding to the two preferential binding modes, for which representative configurations are shown in panels A and B. The basic and polar residues engaged with the membrane (transparent dark-orange surface) are shown as balls and sticks. For clarity the residues in panel B are labelled as follows: R462 (1), R465 (2), K466 (3), S469 (4), N470 (5), K473 (6), N482 (7), K483 (8), T485 (9), S487 (10), and Q489 (11). Colors and representation of the domain as in Fig. 3. For definitions of angles an1 and an2, see Fig. S4.

minima in a region characterized by negative values of cos *an1* and positive values of cos *an2* (Fig. 5 bottom plots). The corresponding configurations showed the interactions between the lipids and the tip of the DEP finger, the N-terminal end of Helix 3, and the C-terminal part of the contiguous loop (Fig. 5 panel A). An alternative binding mode was also observed, where the whole Helix 3 and the contiguous loop, but not the DEP finger, were engaged with the membrane (Fig. 5 panel B). The exceptions were again membranes made of pure POPC or doubly deprotonated POPA, where the domain desorbed or interacted by different binding modes, respectively. Note that the shorter simulation time for systems with POPS:POPE:POPC and POPS:POPA:POPC membranes, led to reduced sampling of the binding orientations.

3.3. Lipid preference

The radial distribution function (RDF) analysis of DEP at binary lipid membranes (see Methods), clearly demonstrates the preference of the domain for the anionic phospholipids over the neutral POPC (Fig. S18). This is further confirmed in Figs. S19 to S21, where the data on contacts, hydrogen bonds, and interaction energies were grouped based on the lipid type. We note from the RDF analysis, that DEP domain bound POPA lipid stronger than POPS and POPG lipids. This observation is in line with the preferential interaction of DEP domain with the phosphate groups, which are fully exposed and accessible on POPA lipids.

A more accurate estimate of the lipid preference was obtained via calculations of the free energy of binding. The starting conformations of DEP domain bound to POPA, POPA:POPC, POPS:POPC, POPS:POPE:POPC, and POPC membranes, were chosen to resemble the binding modes shown in panel A and B of Fig. 5. As summarized in Table 1, DEP domain binds POPA:POPC membrane ~15 kJ mol^{-1} stronger than POPS:POPC membrane, suggesting that POPA is indeed the optimal binding substrate. POPS:POPE:POPC membrane, which mimics the physiological concentration of the most common phospholipids in the inner leaflet of the plasma membranes of human cells [60] was found to be similarly good in binding DEP domain as POPS:POPC mixture, where a higher content of negatively charged lipids was present. Note that strongly binding POPA membrane and more complex POPS:POPE:POPC lipid mixture had large differences/errors in the binding free energy due to the presence of small membrane defects during the pulling, variations in the binding modes and surrounding lipid distribution, and limited simulation time.

3.4. Analysis of DVL3/DEP binding to defined membranes using flow cytometry

To validate the outcome of the MD simulations, we evaluated the binding of DVL3/DEP proteins to lipid vesicles using confocal microscopy and flow cytometry (FC) (Fig. 6A). The vesicles were composed of DOPA, DOPS, and DOPC, as well as POPA, POPS, and POPC lipids (see Methods for details). Halo tag becomes fluorescent upon addition of TMR ligand, which allowed us to observe under the microscope clear binding of Halo-TMR-DVL3 and Halo-TMR-DEP to DOPA vesicles (Fig. 6B). To compare the strength of the protein-membrane interaction, we utilized the FC method, see Fig. 6C. Advantage of FC is the possibility to monitor separately individual events, in this case vesicles, and choose for the analysis only the ones of particular size and density. Moreover, vesicles stained with DiD lipid dye can be clearly distinguished from the debris. Once the FC detection of the vesicles was validated, we optimized the analysis of the protein-vesicles binding. For the optimization we used purified Halo-tagged DVL3 and DOPA vesicles, where we expected the strongest interaction based on microscopy observations.

The results for Halo-TMR-DVL3 and Halo-TMR-DEP with vesicles made of DOPA, DOPS, and DOPC lipids are summarized in Fig. 6D (for raw data and controls see Fig. S5). Both protein constructs bound strongly to DOPA vesicles and weakly to DOPS vesicles, in qualitative agreement with the calculated binding free energies. As expected for a binding mechanism mostly driven by generic electrostatic attraction, no visible interaction was observed with DOPC vesicles. Consistently, decreased amount of anionic phospholipids (i.e. DOPA:DOPC (1:1 mol:mol) mixture) substantially reduced the protein-vesicles association. However, we could not detect any affinity (Fig. S5L) of DEP domain for PIP2:DOPC (1:3 mol:mol) lipid mixture. The same binding trend (i.e. PA > > PS > PC) was reproduced with POPA, POPS, and POPC lipids (Fig. S22). In addition, minor changes in the solution pH (from 8 to 7) enhanced the affinity of DEP domain for DOPA and DOPS vesicles (Fig. 6E), and, only marginally, for DOPA:DOPC (Fig. S23) vesicles, suggesting a possible role of pH in DEP-membrane association.

In summary, these experimental data not only confirm main predictions of MD simulations but also demonstrate a versatile application of FC for the analysis of protein-membrane interactions.

3.5. QCM-D monitoring of DEP domain binding to supported lipid bilayers

The interaction of DEP domain with lipid membranes was independently assessed via quartz crystal microbalance with dissipation monitoring (QCM-D). In short, this technique allows the real-time detection of mass changes at the surface of a piezoelectric sensor oscillating at a specific resonance frequency (*f*). *f* is dependent on the mass of the layer adsorbed onto the sensor surface enabling measurement of the molecule-surface interaction. In our case, the binding of DEP domain to a lipid bilayer formed at the sensor surface would result in a negative frequency change.

QCM-D measurements of DEP domain (without Halo tag) at supported lipid bilayers with composition DOPC, DOPA:DOPC (1:1 mol:mol), DOPS:DOPC (1:1 mol:mol), and PIP2:DOPC (1:3 mol:mol), are shown in Fig. 7. In the presence of anionic phospholipids (DOPA, DOPS, and PIP2), the addition of DEP domain (black arrows) led to a clear decrease in the frequency, revealing specific DEP-membrane binding. In agreement with flow cytometry experiments and simulations, the domain affinity for DOPA lipid was the strongest. As expected, no association of DEP to the neutral DOPC bilayer was detected. The raw data, together with the binding of DEP domain to DOPA:DOPC at different pH conditions, can be found in Figs. S24 and S25, respectively.

Table 1
Free Energy (FE) of binding between DEP domain and membranes with various lipid compositions.

Lipid composition	FE (kJ mol^{-1})[a,b]
POPA	−109.0 ± 18.2
POPA:POPC (1:1)	−73.8 ± 0.3
POPS:POPC (1:1)	−60.9 ± 8.2
POPS:POPE:POPC (7:15:10)	−55.9 ± 26.7
POPC	−23 ± 1.3

[a] Average and standard deviation calculated over both copies of DEP domain.
[b] The bootstrap errors associated with free energy calculation averaged over both copies of the domain are: 4.3, 3.3, 3.1, 4.9, and 1.3 kJ mol^{-1} from top to bottom.

4. Discussion

The interaction of protein effectors with specific phospholipids, such as phosphatidic acid (PA) and phosphatidylserine (PS), plays a crucial role in many biological processes, including cell signaling [61]. In particular, Wnt signaling is regulated by the dynamic relocalization of DVL protein between the plasmamembrane and the cytoplasm [62], a process mediated by the putative interaction of its C-terminal DEP domain with anionic lipids [12,13], especially PA [14]. In our simulations, DEP domain firmly bound to all membranes containing anionic phospholipids, irrespective of their nature and molar concentration. An in-depth analysis of the domain-membrane interaction revealed that the bulk of the hydrogen bonds and interaction energies originates from the

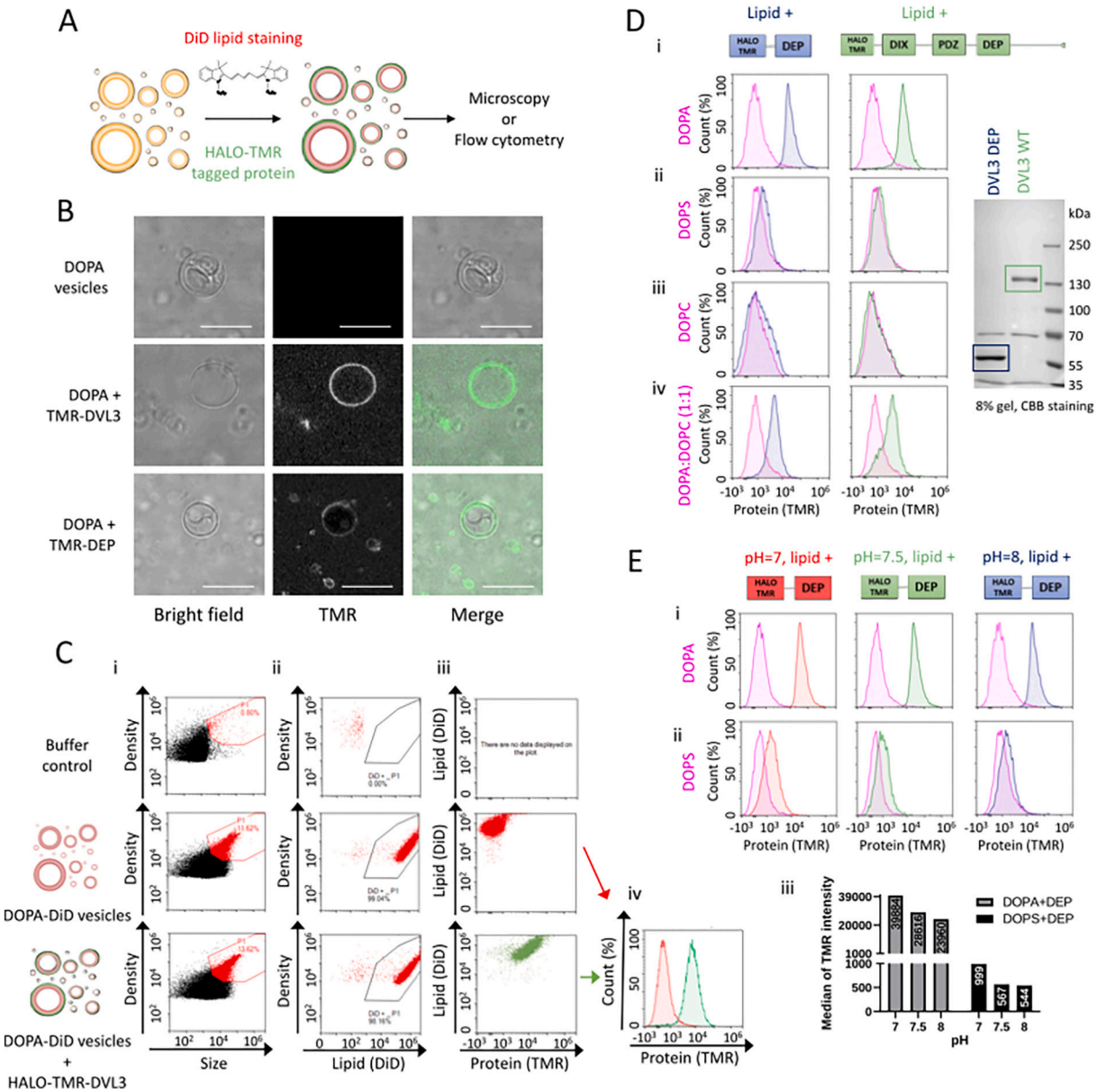

Fig. 6. DEP domain and full length DVL3 binding to the defined synthetic membranes using flow cytometry. (A) Schematic representation of the experimental workflow. Synthetic lipid vesicles were stained with DiD lipid dye and incubated with fluorescently labelled protein. The samples were then analyzed using confocal microscopy (B) or flow cytometry (C). (B) Confocal microscopy images of DOPA vesicles with or without HALO-TMR-DVL3 and HALO-TMR-DEP. Scale bar represents 10 μm. (C) Flow cytometry analysis of DVL3 binding to DOPA vesicles. Gating strategy is shown in dot plots. First, we show size (FSC) vs. density (SSC) gated for vesicles (i), then lipid dye DiD vs. density (SSC) gated for DiD + vesicles (ii), and finally protein label TMR vs. lipid dye DiD (iii). The overlay of TMR channel signals for DOPA-DiD vesicles with and without HALO-TMR-DVL3 is shown in the histogram (iv). Data are shown as normalized count. (D) HALO-TMR-DEP and HALO-TMR-DVL3 binding to vesicles of different composition at pH 8. Histograms show overlay of lipid only and HALO-TMR-DVL3 or HALO-TMR-DEP with DOPA (i), DOPS (ii), DOPC (iii), and DOPA:DOPC 1:1 lipid mixture (iv). Gel with CBB stained purified proteins is shown next to the histograms. (E) HALO-TMR-DEP binding to DOPA (i) or DOPS (ii) lipids at different pH. Histograms show overlay of lipid only and lipid with HALO-TMR-DEP at pH = 7, 7.5, and 8. Graph represents median TMR intensity for each HALO-TMR-DEP + lipid condition with subtracted median intensity of lipid without protein (iii). Raw data and not normalized counts for D and E are shown in Fig. S5. Vesicles schematic used in A and C was created by BioRender.com.

interplay between the basic residues of the domain and the lipid phosphate groups. The particularly strong interaction of DEP domain with the lipid phosphates and the enhanced binding of the domain to PA lipids, shown in a previous work [14] and confirmed by our flow cytometry and QCM-D experiments, indicate that the strength of the electrostatic attraction, responsible for the main recruitment of DEP domain to anionic membranes, is proportional to the availability of the lipid phosphates. Indeed, the domain desorbed from the neutral POPC membrane, where the presence of the bulky and positively charged choline headgroup substituent, makes the phosphate group poorly accessible for electrostatic and hydrogen bond interactions with DEP domain basic residues.

The analysis of the simulations demonstrated that a cluster of lysines and arginines located on Helix 3 and the contiguous loop (R462, R465, K466, K473, and K483) is dominating the interaction with anionic membranes. The identified residues are in perfect agreement with previous reports on DEP domain from DVL2 obtained with a different parametrization [14] and form a basic motif common in peripheral membrane proteins interacting with negatively charged membranes [63–66]. Moreover, the loop contiguous to Helix 3 also accommodates

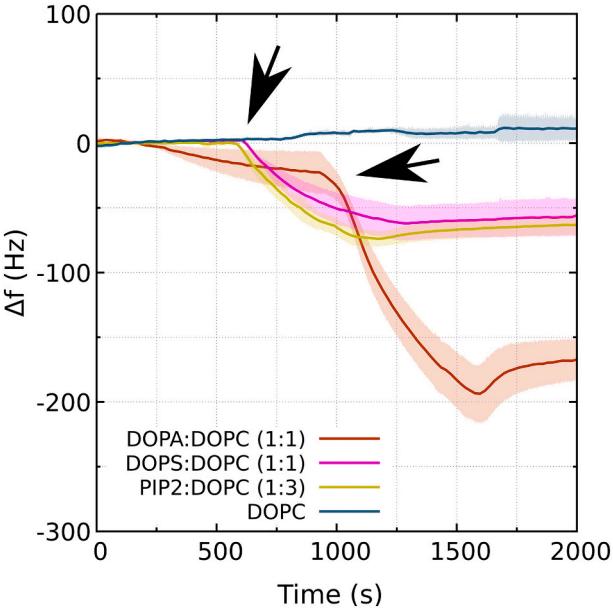

Fig. 7. QCM-D monitoring of DEP domain (without Halo tag) at supported lipid bilayers composed of DOPC, DOPA:DOPC, DOPS:DOPC, and PIP2:DOPC. The binding of the protein to bilayers adsorbed onto the sensor surface results in a negative frequency change, the extent of which is proportional to the amount of the bound protein (i.e. increased binding affinity). For the ease of visualization both x- and y- axes are shifted so that the reference point is represented by the stable lipid bilayer. The data are shown as average (full line) and standard deviation (shaded area) over three separated measurements (see Fig. S25 for raw data). Note that for clarity only the third overtone is considered.

four polar residues (N482, T485, S487, and Q489) that further stabilize the membrane binding, especially in the presence of POPS and POPG lipids (Fig. S26). A third region, known as the tip of the DEP finger (residues 434-LKI-436), was interacting with the membrane more weakly and transiently than Helix3 and the contiguous loop. The interaction was governed by electrostatic attraction and hydrogen bonds involving residue K435, with the support of two preceding arginines, R429 and R431. In addition, few adjacent highly conserved non-polar residues (M432, L434, and I436) and a tryptophane (W433) provided a small but non-negligible contribution to the binding, by means of hydrophobic interactions with the hydrocarbon region of the phospholipids and cation-π interactions with the choline headgroup substituent of POPC, respectively. Notably, both binding mechanisms were observed in other peripheral membrane proteins [67–69].

The dispensable role of the DEP finger in membrane binding was suggested by the description of two preferred binding modes, which differ in (1) the direct contact between the DEP finger and the membrane and (2) the total contribution to the interaction of Helix 3 and the contiguous loop. Both modes occurred with similar probability and were separated by a small energy barrier of ~5 kJ mol^{-1}, which is available in the thermal energy of the system at 310 K. Indeed, we observed a full transition from one mode to the other during our simulations in a sort of rocking motion (see Video S1). Note that DEP domain was binding differently to membranes with doubly deprotonated POPA lipids. The presence of cation-mediated clustering of POPA headgroups (Fig. S27), similarly observed in previous simulations [70], led to unusual electrostatic interactions of the N-terminus of DEP domain or to defects of the membrane surface, where the side chain of the apolar residues populating the DEP finger favorably inserted (Fig. S28).

In all our simulations and experiments DEP domain showed a consistent preference for PA lipids over PS. However, the preference was considerably less pronounced in simulations. To reconcile our observations, we note that non-polarizable force fields tend to overestimate the electrostatic interaction between charged groups [71]. Thus, in our systems, the excessive adsorption of solution cations to phospholipid membranes [72,73] would result in electrostatic screening of DEP-membrane interaction, an effect enhanced by PC and PS headgroup substituent. Yet, as demonstrated by the non-negligible free energy of binding of DEP domain at the neutral POPC membrane (see Table 1), also the affinity of DEP basic motif for the lipid phosphates could be exaggerated. Moreover, during our free energy calculations the molecular charge of each POPA lipid remained fixed at −1e (i.e. singly deprotonated), despite the fact that its second pK_a is in the physiological pH range [19]. On the contrary, the flow cytometry and QCM-D experiments shown in Figs. 6D and 7 were performed at pH 8, condition at which a portion of the PA lipids is fully deprotonated leading to charge −2e. The extent of the deprotonation can be amplified by specific protein-PA interactions, as predicted by the electrostatic/hydrogen bond mechanism [74]. Thus, with respect to experiments, the POPA model used in simulations may underestimate the magnitude of the electrostatic attraction existing between DEP and PA lipids.

The selectivity of DEP domain between PS and PG lipids is not straightforward. Despite the identical molecular charge and similar hydrogen bond propensity, POPS and POPG interacted with DEP domain in different ways. The glycerol of POPG headgroup was oriented parallel to the membrane plane [75], which made its phosphate groups more accessible for electrostatic interactions with DEP domain. This effect was only partially compensated by the higher number of hydrogen bonds and total interaction energy existing between the domain and the headgroup substituent of POPS (Figs. S20 and S21), leading to an overall preference for POPG over POPS lipid (see Fig. S18).

Finally, we comment on the employed experimental methodologies. Flow cytometry (FC) evaluates protein-lipid interaction in a more physiological context compared with QCM-D monitoring (i.e. vesicles in suspension vs supported lipid bilayers (SLBs)). While QCM-D is a label-free technology, FC requires the coupling of DVL3/DEP constructs with Halo tag. Although Halo alone shows no affinity for DOPA vesicles (Fig. S29), its overall negative charge in the explored pH range might decrease the sensitivity towards low affinity anionic lipids (weak and no binding to PS and PIP2 vesicles, respectively). Nevertheless, we emphasize that the independent findings from both FC and QCM-D are in general agreement and provide a strong evidence on DEP domain lipid preference.

4.1. Biological consequences

Functional and microscopy experiments demonstrated that DEP domain is required for the activation of Wnt signaling [8] and the co-localization of DVL protein with Frizzled receptor to the plasma membrane [76,77]. Here, we show that DEP domain adsorb to membranes containing negatively charged lipids mainly via electrostatic attraction, with a strong preference for PA over PS lipids. Therefore, we hypothesize that the weak interaction between DEP domain and the abundant PS lipids, could lead to the transient translocation of DVL protein from the cytoplasm to the inner leaflet of the plasma membrane. In response to local increase of PA concentration, for example due to de novo biosynthesis [78] and mechanical stimulation [79], the membrane binding would stabilize, facilitating the direct interaction of DVL with Frizzled receptor and the initiation of the signal transduction. The increase of PA local concentration could potentially be very small, as suggested by simulations with POPA:POPC membrane, where approximately 5 PA lipids were in close contact with DEP domain (Fig. S18). However, in flow cytometry experiments with DOPA:DOPC (1:1) and pure DOPA vesicles, we observed that the binding is dependent on the concentration of the anionic lipid (Fig. 6D), thus further increase in PA concentration would consolidate the association. Consistent results were provided by our free energy calculations, where the binding to POPA membrane was ~30 kJ mol^{-1} stronger than to POPA:POPC (1:1) membrane (Table 1).

The preferred interaction of DEP with the lipid phosphates also

suggests that phosphoinositides, another family of functionally active phospholipids with available phosphate groups [80], could contribute to DEP/DVL binding, as was similarly reported for MARCKS protein [81,82]. QCM-D measurements summarized in Fig. 7 indicate that DEP domain binds bilayers containing PIP2, with similar strength as DOPS: DOPC (1:1) but significantly weaker than DOPA:DOPC (1:1) bilayers. The binding of DEP domain to PIP2 lipids is in line with previous experiments showing the essential role of PIP2 and two kinases sequentially producing PIP2 (PI4KII and PIP5K) in Wnt/β-catenin signaling at the level of DVL protein [83]. Subsequent work proved that AMER1, a protein recognizing phosphoinositides, links FZD/DVL complex with downstream LRP6/Axin module [84,85]. Local production of PIP2 directly resulting in stronger DVL membrane interaction, thus represents the attractive possibility explaining proximal events in the Wnt signal transduction.

Moreover, the electrostatic nature of DEP-membrane interaction makes the binding pH and salt concentration dependent (Fig. 6E), which provides the potential for further regulation of DVL-membrane association. However, the effect could be complex and system dependent. In our experiments, the pH effect was minimal for both DEP domain binding to DOPA:DOPC (1:1) vesicles (Fig. S23) and SLBs (Fig. S25), while a similar, but not identical, DEP domain from DVL2 was previously reported to significantly decrease the binding at acidic pH [14]. Therefore, additional work is necessary to understand the sensitivity of DEP-membrane association to changes in the local environment.

The analysis of the alternative binding modes revealed that the DEP finger is partially dispensable for membrane binding and it can be involved in other functions, e.g. interaction with Frizzled receptor [10,76] or DEP oligomerization [11]. Interestingly, binding with alternative orientations was also reported for other mammalian [86] and bacterial [87] peripheral membrane proteins.

Finally, we emphasize that we needed higher concentration of DEP domain compared to full-length DVL to show membrane binding in our flow cytometry measurements (Fig. 6D). This difference indicates that, despite DEP domain plays a crucial role in membrane binding, other regions of DVL could be cooperatively involved in this process and/or that significant intramolecular changes are necessary for DEP domain to optimally carry out its function.

5. Conclusion

The identification of the protein residues and physical forces driving the protein-membrane interaction is essential for understanding the mechanism of action and regulation of many biological processes [88,89].

By combining MD simulations with flow cytometry and QCM-D experiments, we demonstrate that the C-terminal DEP domain from DVL protein in Wnt signaling pathway favorably interacts with all the investigated anionic model membranes, especially those containing PA lipids. The interaction is mainly driven by the electrostatic attraction between a cluster of positively charged residues on DEP domain and the negatively charged lipid phosphate groups. The observed strong preference for PA lipids together with the weaker binding to PS and PIP2 lipids, may shed light on yet unclear regulatory aspects of Wnt signaling and also pave the way for a more profound comprehension of the complex protein-membrane interplay.

Author contributions

R.V. designed the research. F.L.F. carried out all simulations, analyzed the data. M.K. performed microscopy and flow cytometry experiments. M.D. carried out QCM-D measurements. P.P. and M.K. produced and purified proteins. F.L.F., R.V., V.B., M.K., and M.D. wrote the article.

Declaration of competing interest

The authors declare that they have no known competing financial interests or personal relationships that could have appeared to influence the work reported in this paper.

Acknowledgments

This work was supported by the Czech Science Foundation (grant GA20-20152S and GA22-25365S) and the European Research Council (ERC) under the European Union's Horizon 2020 research and innovation programme (grant agreement No 101001470). Computational resources were provided by the CESNET LM2015042 and the CERIT Scientific Cloud LM2015085 provided under the program Projects of Large Research, Development, and Innovations Infrastructures. Additional computational resources were obtained from IT4 Innovations National Supercomputing Center – LM2015070 project supported by MEYS CR from the Large Infrastructures for Research, Experimental Development and Innovations.

Appendix A. Supplementary data

Supplementary data to this article can be found online at https://doi.org/10.1016/j.bbamem.2022.183983.

References

[1] H. Clevers, R. Nusse, Wnt/β-catenin signaling and disease, Cell 149 (2012) 1192–1205.
[2] N. Ghosh, U. Hossain, A. Mandal, P.C. Sil, The wnt signaling pathway: a potential therapeutic target against cancer, Ann. N. Y. Acad. Sci. 1443 (2019) 54–74.
[3] R. Jackstadt, M.C. Hodder, O.J. Sansom, Wnt and β-catenin in cancer: genes and therapy, Annu.Rev.Cancer Biol. 4 (2020) 177–196.
[4] M.V. Semenov, R. Habas, B.T. MacDonald, X. He, Snapshot: noncanonical wnt signaling pathways, Cell 131 (2007) 1378.e1–1378.e2.
[5] S. Angers, R.T. Moon, Proximal events in wnt signal transduction, Nat. Rev. Mol. Cell Biol. 10 (2009) 468–477.
[6] M. Sharma, I. Castro-Piedras, G.E. Simmons, K. Pruitt, Dishevelled: a masterful conductor of complex wnt signals, Cell. Signal. 47 (2018) 52–64.
[7] A. Kafka, S. Bašić-Kinda, N. Pećina-Šlaus, The cellular story of dishevelleds, Croat. Med.J. 55 (2014) 459–46667.
[8] P. Paclíková, O. Bernatík, T.W. Radaszkiewicz, V. Bryja, The n-terminal part of the dishevelled dep domain is required for wnt/β-catenin signaling in mammalian cells, Mol. Cell. Biol. 37 (2017), e00145–17.
[9] M.V. Gammons, T.J. Rutherford, Z. Steinhart, S. Angers, M. Bienz, Essential role of the dishevelled dep domain in a wnt-dependent human-cell-based complementation assay, J. Cell Sci. 129 (2016) 3892–3902.
[10] D.V.F. Tauriello, I. Jordens, K. Kirchner, J.W. Slootstra, T. Kruitwagen, B.A. M. Bouwman, M. Noutsou, S.G.D. Rudiger, K. Schwamborn, A. Schambony, M. M. Maurice, Wnt/-catenin signaling requires interaction of the dishevelled dep domain and c terminus with a discontinuous motif in frizzled, Proc. Natl. Acad. Sci. 109 (2012) E812–E820.
[11] M. Gammons, M. Renko, C. Johnson, T. Rutherford, M. Bienz, Wnt signalosome assembly by dep domain swapping of dishevelled, Mol. Cell 64 (2016) 92–104.
[12] H. Wong, J. Mao, J. Nguyen, S. Srinivas, W. Zhang, B. Liu, L. Li, D. Wu, J. Zheng, Structural basis of the recognition of the dishevelled dep domain in he wnt signaling pathway, Nat. Struct. Biol. 7 (2000) 1178–1184.
[13] M. Simons, W.J. Gault, D. Gotthardt, R. Rohatgi, T.J. Klein, Y. Shao, H.-J. Lee, A.-L. Wu, Y. Fang, L.M. Satlin, J.T. Dow, J. Chen, J. Zheng, M. Boutros, M. Mlodzik, Electrochemical cues regulate assembly of the frizzled/dishevelled complex at the plasma membrane during planar epithelial polarization, Nat. Cell Biol. 11 (2009) 286–294.
[14] D. Capelluto, X. Zhao, A. Lucas, J. Lemkul, S. Xiao, X. Fu, F. Sun, D. Bevan, C. Finkielstein, Biophysical and molecular-dynamics studies of phosphatidic acid binding by the dvl-2 dep domain, Biophys. J. 106 (2014) 1101–1111.
[15] G.V. Meer, D.R. Voelker, G.W. Feigenson, Membrane lipids: where they are and how they behave, Nat. Rev. Mol. Cell Biol. 9 (2008) 112–124.
[16] D. Casares, P.V. Escribá, C.A. Rosselló, Membrane lipid composition: effect on membrane and organelle structure, function and compartmentalization and therapeutic avenues, Int. J. Mol. Sci. 20 (2019) 2167.
[17] S.V. Consonni, M.M. Maurice, J.L. Bos, Dep domains: structurally similar but functionally different, Nat. Rev. Mol. Cell Biol. 15 (2014) 357–362.
[18] J. Li, X. Wang, T. Zhang, C. Wang, Z. Huang, X. Luo, Y. Deng, A review on phospholipids and their main applications in drug delivery systems, Asian Journal of Pharmaceutical Sciences 10 (2015) 81–98.
[19] E.E. Kooijman, K.N. Burger, Biophysics and function of phosphatidic acid: a molecular perspective, Biochimica et biophysica acta (BBA) - molecular and cell biology ofLipids 1791 (2009) 881–888.

[20] T. Zhang, S.L. Brantley, D. Verreault, R. Dhankani, S.A. Corcelli, H.C. Allen, Effect of ph and salt on surface pKa of phosphatidic acid monolayers, Langmuir 34 (2018) 530–539.
[21] S. Jo, T. Kim, V.G. Iyer, W. Im, Charmm-gui: a web-based graphical user interface for charmm, J. Comput. Chem. 29 (2008) 1859–1865.
[22] B.R. Brooks, C.L. Brooks, A.D. Mackerell, L. Nilsson, R.J. Petrella, B. Roux, Y. Won, G. Archontis, C. Bartels, S. Boresch, A. Caflisch, L. Caves, Q. Cui, A.R. Dinner, M. Feig, S. Fischer, J. Gao, M. Hodoscek, W. Im, K. Kuczera, T. Lazaridis, J. Ma, V. Ovchinnikov, E. Paci, R.W. Pastor, C.B. Post, J.Z. Pu, M. Schaefer, B. Tidor, R. M. Venable, H.L. Woodcock, X. Wu, W. Yang, D.M. York, M. Karplus, Charmm: the biomolecular simulation program, J. Comput. Chem. 30 (2009) 1545–1614.
[23] J. Lee, X. Cheng, J.M. Swails, M.S. Yeom, P.K. Eastman, J.A. Lemkul, S. Wei, J. Buckner, J.C. Jeong, Y. Qi, S. Jo, V.S. Pande, D.A. Case, C.L. Brooks, A. D. MacKerell, J.B. Klauda, W. Im, Charmm-gui input generator for namd, gromacs, amber, openmm, and charmm/openmm simulations using the charmm36 additive force field, J. Chem. Theory Comput. 12 (2016) 405–413.
[24] A. Yu, Y. Xing, S.C. Harrison, T. Kirchhausen, Structural analysis of the interaction between dishevelled2 and clathrin ap-2 adaptor, a critical step in noncanonical wnt signaling, Structure 18 (2010) 1311–1320.
[25] L. Schrödinger, W. DeLano, Pymol, URL: http://www.pymol.org/pymol, 2020.
[26] T.J. Dolinsky, J.E. Nielsen, J.A. McCammon, N.A. Baker, Pdb2pqr: an automated pipeline for the setup of Poisson-Boltzmann electrostatics calculations, Nucleic Acids Res. 32 (2004) W665–W667.
[27] N.A. Baker, D. Sept, S. Joseph, M.J. Holst, J.A. McCammon, Electrostatics of nanosystems: application to microtubules and the ribosome, Proc. Natl. Acad. Sci. 98 (2001) 10037–10041.
[28] W.L. Jorgensen, J. Chandrasekhar, J.D. Madura, R.W. Impey, M.L. Klein, Comparison of simple potential functions for simulating liquid water, J. Chem. Phys. 79 (1983) 926–935.
[29] B. Hess, H. Bekker, H.J.C. Berendsen, J.G.E.M. Fraaije, Lincs: a linear constraint solver for molecular simulations, J. Comput. Chem. 18 (1997) 1463–1472.
[30] S. Miyamoto, P.A. Kollman, Settle: an analytical version of the shake and rattle algorithm for rigid water models, J. Comput. Chem. 13 (1992) 952–962.
[31] T. Darden, D. York, L. Pedersen, Particle mesh ewald: an nlog(n) method for ewald sums in large systems, J. Chem. Phys. 98 (1993) 10089–10092.
[32] G. Bussi, D. Donadio, M. Parrinello, Canonical sampling through velocity rescaling, J. Chem. Phys. 126 (2007), 014101.
[33] M. Parrinello, A. Rahman, Polymorphic transitions in single crystals: a new molecular dynamics method, J. Appl. Phys. 52 (1981) 7182–7190.
[34] G. Patey, J. Valleau, The free energy of spheres with dipoles: Monte Carlo with multistage sampling, Chem. Phys. Lett. 21 (1973) 297–300.
[35] G.M. Torrie, J.P. Valleau, Monte Carlo free energy estimates using non-boltzmann sampling: application to the sub-critical lennard-jones fluid, Chem. Phys. Lett. 28 (1974) 578–581.
[36] G. Torrie, J. Valleau, Nonphysical sampling distributions in Monte Carlo free-energy estimation: umbrella sampling, J. Comput. Phys. 23 (1977) 187–199.
[37] S. Kumar, J.M. Rosenberg, D. Bouzida, R.H. Swendsen, P.A. Kollman, The weighted histogram analysis method for free-energy calculations on biomolecules. i. The method, J. Comput. Chem. 13 (1992) 1011–1021.
[38] D. Van Der Spoel, E. Lindahl, B. Hess, G. Groenhof, A.E. Mark, H.J.C. Berendsen, Gromacs: fast, flexible, and free, J. Comput. Chem. 26 (2005) 1701–1718.
[39] M.J. Abraham, T. Murtola, R. Schulz, S. Páll, J.C. Smith, B. Hess, E. Lindahl, Gromacs: high performance molecular simulations through multi-level parallelism from laptops to supercomputers, SoftwareX 1 (2015) 19–25.
[40] K. Lindorff-Larsen, S. Piana, K. Palmo, P. Maragakis, J.L. Klepeis, R.O. Dror, D. E. Shaw, Improved side-chain torsion potentials for the amber ff99sb protein force field, Proteins: Struct.Funct.Bioinforma. 78 (8) (2010) 1950–1958.
[41] J.P.M. Jämbeck, A.P. Lyubartsev, An extension and further validation of an all-atomistic force field for biological membranes, J.Chem.Theory Comput.8 8 (2012) 2938–2948.
[42] J.P.M. Jämbeck, A.P. Lyubartsev, Derivation and systematic validation of a refined all-atom force field for phosphatidylcholine lipids, Journal of Physical Chemistry B 116 (2012) 3164–3179.
[43] J.P.M. Jämbeck, A.P. Lyubartsev, Another piece of the membrane puzzle: extending slipids further, J. Chem. Theory Comput. 9 (2013) 774–784.
[44] J.B. Klauda, R.M. Venable, J.A. Freites, J.W. O'Connor, D.J. Tobias, C. Mondragon-Ramirez, I. Vorobyov, A.D. MacKerell, R.W. Pastor, Update of the charmm all-atom additive force field for lipids: validation on six lipid types, J. Phys. Chem. B 114 (2010) 7830–7843.
[45] A.D. Becke, Density-functional thermochemistry. iii. The role of exact exchange, J. Chem. Phys. 98 (1993) 5648–5652.
[46] C. Lee, W. Yang, R.G. Parr, Development of the colle-salvetti correlation-energy formula into a functional of the electron density, Phys. Rev. B 37 (1988) 785–789.
[47] P.J. Stephens, F.J. Devlin, C.F. Chabalowski, M.J. Frisch, Ab initio calculation of vibrational absorption and circular dichroism spectra using density functional force fields, J. Phys. Chem. 98 (1994) 11623–11627.
[48] E. Miliordos, S.S. Xantheas, On the validity of the basis set superposition error and complete basis set limit extrapolations for the binding energy of the formic acid dimer, J. Chem. Phys. 142 (2015), 094311.
[49] C.I. Bayly, P. Cieplak, W. Cornell, P.A. Kollman, A well-behaved electrostatic potential based method using charge restraints for deriving atomic charges: the resp model, J. Phys. Chem. 97 (1993) 10269–10280.
[50] J. Tomasi, B. Mennucci, E. Cancès, The ief version of the pcm solvation method: an overview of a new method addressed to study molecular solutes at the qm ab initio level, J. Mol. Struct. THEOCHEM 464 (1999) 211–226.
[51] C.S. Pomelli, J. Tomasi, V. Barone, An improved iterative solution to solve the electrostatic problem in the polarizable continuum model, Theor.Chem.Acc. 105 (2001) 446–451.
[52] U.C. Singh, P.A. Kollman, An approach to computing electrostatic charges for molecules, J. Comput. Chem. 5 (1984) 129–145.
[53] M.J. Frisch, G.W. Trucks, H.B. Schlegel, G.E. Scuseria, M.A. Robb, J.R. Cheeseman, G. Scalmani, V. Barone, G.A. Petersson, H. Nakatsuji, X. Li, M. Caricato, A. V. Marenich, J. Bloino, B.G. Janesko, R. Gomperts, B. Mennucci, H.P. Hratchian, J. V. Ortiz, A.F. Izmaylov, J.L. Sonnenberg, D. Williams-Young, F. Ding, F. Lipparini, F. Egidi, J. Goings, B. Peng, A. Petrone, T. Henderson, D. Ranasinghe, V. G. Zakrzewski, J. Gao, N. Rega, G. Zheng, W. Liang, M. Hada, M. Ehara, K. Toyota, R. Fukuda, J. Hasegawa, M. Ishida, T. Nakajima, Y. Honda, O. Kitao, H. Nakai, T. Vreven, K. Throssell, J.A. Montgomery Jr., J.E. Peralta, F. Ogliaro, M. J. Bearpark, J.J. Heyd, E.N. Brothers, K.N. Kudin, V.N. Staroverov, T.A. Keith, R. Kobayashi, J. Normand, K. Raghavachari, A.P. Rendell, J.C. Burant, S.S. Iyengar, J. Tomasi, M. Cossi, J.M. Millam, M. Klene, C. Adamo, R. Cammi, J.W. Ochterski, R.L. Martin, K. Morokuma, O. Farkas, J.B. Foresman, D.J. Fox, Gaussian 16 Revision B.01, Wallingford, CT (2016).
[54] J. Wang, R.M. Wolf, J.W. Caldwell, P.A. Kollman, D.A. Case, Development and testing of a general amber force field, J. Comput. Chem. 25 (2004) 1157–1174.
[55] J. Wang, W. Wang, P.A. Kollman, D.A. Case, Automatic atom type and bond type perception in molecular mechanical calculations, J. Mol. Graph. Model. 25 (2006) 247–260.
[56] W. Humphrey, A. Dalke, K. Schulten, VMD – visual molecular dynamics, J. Mol. Graph. 14 (1996) 33–38.
[57] D. Frishman, P. Argos, Knowledge-based secondary structure assignment, Proteins Struct. Funct. Genet. 23 (1995) 566–579.
[58] G.A. Tribello, M. Bonomi, D. Branduardi, C. Camilloni, G. Bussi, Plumed 2: new feathers for an old bird, Comput. Phys. Commun. 185 (2014) 604–613.
[59] S.R. Tabaei, J.-H. Choi, G. Haw Zan, V.P. Zhdanov, N.-J. Cho, Solvent-assisted lipid bilayer formation on silicon dioxide and gold, Langmuir 30 (2014) 10363–10373.
[60] T. Fujimoto, I. Parmryd, Interleaflet coupling, pinning, and leaflet asymmetry—major players in plasma membrane nanodomain formation, Front. Cell Dev.Biol. 4 (2017).
[61] C.L. Stace, N.T. Ktistakis, in: Phosphatidic acid- and phosphatidylserine-binding proteins, Biochimica et Biophysica Acta (BBA), Molecular and Cell Biology of Lipids 1761, Lipid-Binding Domains, 2006, pp. 913–926.
[62] M. Mlodzik, The dishevelled protein family, in: Current Topics in Developmental Biology volume 117, Elsevier, 2016, pp. 75–91.
[63] S. Takahashi, P.M. Pryciak, Identification of novel membrane-binding domains in multiple yeast cdc42 effectors, Mol. Biol. Cell 18 (2007) 4945–4956.
[64] G. Kaur, A. Pinggera, N.J. Ortner, A. Lieb, M.J. Sinnegger-Brauns, V. Yarov-Yarovoy, G.J. Obermair, B.E. Flucher, J. Striessnig, A polybasic plasma membrane binding motif in the i–ii linker stabilizes voltage-gated cav1.2 calcium channel function, J. Biol. Chem. 290 (2015) 21086–21100.
[65] I.C.R. Barbosa, H. Shikata, M. Zourelidou, M. Heilmann, I. Heilmann, C. Schwechheimer, Phospholipid composition and a polybasic motif determine d6 protein kinase polar association with the plasma membrane and tropic responses, Development 143 (2016) 4687–4700.
[66] V. Papayannopoulos, C. Co, K.E. Prehoda, S. Snapper, J. Taunton, W.A. Lim, A polybasic motif allows n-wasp to act as a sensor of pip2 density, Mol. Cell 17 (2005) 181–191.
[67] Q. Waheed, H.M. Khan, T. He, M. Roberts, A. Gershenson, N. Reuter, Interfacial aromatics mediating cation-π interactions with choline-containing lipids can contribute as much to peripheral protein affinity for membranes as aromatics inserted below the phosphates, J.Phys.Chem.Lett. 10 (2019) 3972–3977.
[68] A. Whited, A. Johs, The interactions of peripheral membrane proteins with biological membranes, Chem. Phys. Lipids 192 (2015) 51–59.
[69] A.L. Lomize, I.D. Pogozheva, M.A. Lomize, H.I. Mosberg, The role of hydrophobic interactions in positioning of peripheral proteins in membranes, BMC Struct. Biol. 7 (2007) 44.
[70] U. Kwolek, W. Kulig, P. Wydro, M. Nowakowska, T. Róg, M. Kepczynski, Effect of phosphatidic acid on biomembrane: experimental and molecular dynamics simulations study, J. Phys. Chem. B 119 (2015) 10042–10051.
[71] E. Duboué-Dijon, M. Javanainen, P. Delcroix, P. Jungwirth, H. Martinez-Seara, A practical guide to biologically relevant molecular simulations with charge scaling for electronic polarization, J. Chem. Phys. 153 (2020), 050901.
[72] J. Melcr, H. Martinez-Seara, R. Nencini, J. Kolafa, P. Jungwirth, O.H.S. Ollila, Accurate binding of sodium and calcium to a POPC bilayer by effective inclusion of electronic polarization, J. Phys. Chem. B 122 (2018) 4546–4557.
[73] J. Melcr, T.M. Ferreira, P. Jungwirth, O.H.S. Ollila, Improved cation binding to lipid bilayers with negatively charged POPS by effective inclusion of electronic polarization, J. Chem. Theory Comput. 16 (2020) 738–748.
[74] E.E. Kooijman, D.P. Tieleman, C. Testerink, T. Munnik, D.T. Rijkers, K.N. Burger, B. de Kruijff, An electrostatic/hydrogen bond switch as the basis for the specific interaction of phosphatidic acid with proteins, J. Biol. Chem. 282 (2007) 11356–11364.
[75] N. Kučerka, B.W. Holland, C.G. Gray, B. Tomberli, J. Katsaras, Scattering density profile model of popg bilayers as determined by molecular dynamics simulations and small-angle neutron and x-ray scattering experiments, J. Phys. Chem. B 116 (2012) 232–239.
[76] J.D. Axelrod, J.R. Miller, J.M. Shulman, R.T. Moon, N. Perrimon, Differential recruitment of Dishevelled provides signaling specificity in the planar cell polarity and wingless signaling pathways, Genes Dev. 12 (1998) 2610–2622.

[77] W.J. Pan, S.Z. Pang, T. Huang, H.Y. Guo, D. Wu, L. Li, Characterization of function of three domains in dishevelled-1: dep domain is responsible for membrane translocation of dishevelled-1, Cell Res. 14 (2004) 324–330.
[78] J. Cai, H. Abramovici, S.H. Gee, M.K. Topham, Diacylglycerol kinases as sources of phosphatidic acid, Biochim. Biophys. Acta (BBA) - Mol. Cell Biol. Lipids 1791 (2009) 942–948. Phospholipase D.
[79] S.-S. Lin, Y.-W. Liu, Mechanical stretch induces mtor recruitment and activation at the phosphatidic acid-enriched macropinosome in muscle cell, Front.Cell Dev.Biol. 7 (2019).
[80] E.J. Dickson, B. Hille, Understanding phosphoinositides: rare, dynamic, and essential membrane phospholipids, Biochem. J. 476 (2019) 1–23.
[81] W. Zhang, E. Crocker, S. McLaughlin, S.O. Smith, Binding of peptides with basic and aromatic residues to bilayer membranes: phenyalanine in the myristoylated alanine-rich c kinase substrate effector domain penetrates into the hydrophobic core of the bilayer, J. Biol. Chem. 278 (2003) 21459–21466.
[82] J. Wang, A. Arbuzova, G. Hangyás-Mihályné, S. McLaughlin, The effector domain of myristoylated alanine-rich c kinase substrate binds strongly to phosphatidylinositol 4,5-bisphosphate, J. Biol. Chem. 276 (2001) 5012–5019.
[83] W. Pan, S.-C. Choi, H. Wang, Y. Qin, L. Volpicelli-Daley, L. Swan, L. Lucast, C. Khoo, X. Zhang, L. Li, C.S. Abrams, S.Y. Sokol, D. Wu, Wnt3a-mediated formation of phosphatidylinositol 4,5-bisphosphate regulates lrp6 phosphorylation, Science 321 (2008) 1350–1353.
[84] K. Tanneberger, A.S. Pfister, K. Brauburger, J. Schneikert, M.V. Hadjihannas, V. Kriz, G. Schulte, V. Bryja, J. Behrens, Amer1/wtx couples wnt-induced formation of ptdins(4,5)p to lrp6 phosphorylation: Amer1 regulates lrp6 phosphorylation, EMBO J. 30 (2011) 1433–1443.
[85] V. Kříž, V. Pospíchalová, J. Mašek, M.B.C. Kilander, J. Slavík, K. Tanneberger, G. Schulte, M. Machala, A. Kozubík, J. Behrens, V. Bryja, β-arrestin promotes wnt-induced low density lipoprotein receptor-related protein 6 (lrp6) phosphorylation via increased membrane recruitment of amer1 protein, J. Biol. Chem. 289 (2014) 1128–1141.
[86] M. Alwarawrah, J. Wereszczynski, Investigation of the effect of bilayer composition on pkcα-c2 domain docking using molecular dynamics simulations, J. Phys. Chem. B 121 (2017) 78–88.
[87] N. Labajová, N. Baranova, M. Jurásek, R. Vácha, M. Loose, I. Barák, Cardiolipin-containing lipid membranes attract the bacterial cell division protein diviva, Int. J. Mol. Sci. 22 (2021) 8350.
[88] W. Cho, R.V. Stahelin, Membrane-protein interactions in cell signaling and membrane trafficking, Annu. Rev. Biophys. Biomol. Struct. 34 (2005) 119–151.
[89] H. Yin, A.D. Flynn, Drugging membrane protein interactions, Annu. Rev. Biomed. Eng. 18 (2016) 51–76.